CHEMICAL ENGINEERING TRANSACTIONS
VOL. 70, 2018
A publication of AIDIC
The Italian Association of Chemical Engineering
Online at www.aidic.it/cet
Guest Editors: Timothy G. Walmsley, Petar S. Varbanov, Rongxin Su, Jiří J. Klemeš

ISBN 978-88-95608-67-9; **ISSN** 2283-9216
DOI: 10.3303/CET1870183

Evaluation of Corrosion Damage Obtained During the Combustion Process in a Boiler. Case Study: Ferritic Steel ASTM A335 P91

Anibal Alviz-Meza[a]*, Viatcheslav Kafarov[a], Dario Y. Peña-Ballesteros[b]

[a]Centro de Investigación para el Desarrollo Sostenible en Industria y Energía, Universidad Industrial de Santander, Bucaramanga, Colombia. Ciudad Universitaria, Cr 27 #9, A.A. 680002
[b]Grupo de Investigación en Corrosión, Universidad Industrial de Santander, Bucaramanga, Colombia. Parque Tecnológico Guatiguará, Piedecuesta, A.A. 681011
anibalalvizm@hotmail.com

The corrosive effects developed on Fe-9Cr-1Mo steel in a typical combustion environment were evaluated. For this, steel samples were submitted in a pirotubular horizontal boiler, through the design of a coupon holder. With the experimental conditions characterized, the theoretical corrosion products were simulated; which showed similarity with SEM-EDS and DRX analysis, in the formation of hematite, magnetite and chromite. On the other hand, the oxide layers morphology deposited on the substrate, indicated the appearance of multiple efforts in them: cracks, pores, voids and detachments were observed. To complement these observations, the kinetic study was carried out, which allowed to determine a semi-protective behaviour from the oxide layers formed on Fe-9Cr-1Mo steel; where the diffusive processes are partially reduced. Finally, only oxidation and some localized nitridation could be identified. Carburization could not be identified due to the high oxygen potentials in the environment, and to the short-selected exposure times.

1. Introduction

The use of ferritic steel such as Fe-9Cr-1Mo (P91) is very common in industrial equipment, which require alloys with good mechanical properties and acceptable corrosion resistance at high temperatures. This alloy is a Cr-Mo martensitic steel, with small additions of V, Nb and N that are useful to stabilize carbides and carbonitrides, improving steel creep and fatigue resistance. However, researchers such as Fabricius and Jackson (2016) have collected several cases of premature failure of this alloy during its service in heaters, superheaters and steam generators. The main reported failures are: local stress raisers and reduction of creep strength; which appear for poor alloy designs or for its use outside design specifications. These reports indicate that P91 steel approaches to its creep and tensile strength limits around 700 ºC. Moreover, regard to corrosion resistance, the fusion of typical P91 oxides like MnO_2, can be produced at 550 ºC, suggesting a limit for catastrophic corrosion.

Regarding to P91 corrosion resistance in real conditions, there is little information available, however in a study carried out by Ju et al. (1997), this alloy showed an unusual failure due to carburization and hydrogen attack in a feed furnace of dehydrogenation unit, in linear alkyl benzene plant. The analysis carried out by them, showed attacks by pitting and cracking in the extracted tubes.

On the other hand, there are the studies carried out in simulated combustion environments, where researchers like Peña-Ballesteros et al. (2012) and Alviz et al. (2017a) reported different corrosion effects. Peña-Ballesteros et al. (2012) demonstrated that in reduced combustion atmospheres, such as CH_4, CO, CO_2 and H_2, at 550, 650 and 750 ºC, it is possible to obtain carburization an oxidation simultaneously. While, Alviz et al. (2017a) observed that in an atmosphere rich in oxygen, carburization effect is suppressed, for the CO_2-O_2-N_2-H_2O-H_2S combustion environment at 750 ºC.

Moreover, researchers such as Martinelli et al. (2015) and Rouillard and Furukawa (2016) have studied carburization in other reduced oxygen environments, noting that in pure CO_2 is also possible to obtain internal carburization on P91 steel at 550 and 600 ºC.

Please cite this article as: Alviz-Meza A., Kafarov V., Pena-Ballesteros D.Y., 2018, Evaluation of corrosion damage obtained during the combustion process in a boiler. case study: ferritic steel astm a335 p91 , Chemical Engineering Transactions, 70, 1093-1098 DOI:10.3303/CET1870183

Carburization and oxidation are the most important corrosion effects at high temperatures, which can promote changes in the properties of P91 steel in a combustion environment without H_2S; the first affecting ductility and thermofluence of the alloy, and the second creating oxide layers to difficult ionic diffusion through the oxide/gas interface. However, in the scientific literature there is little information about corrosion in real and simulated combustion environments, reason under which the present research work was based.
Finally, this research follows the lines of the studies realized by Kafarov et al. (2015), where the eco-efficiency of the combustion process in a refinery was evaluated, having in consideration CO_2 emission and the adiabatic temperature in a furnace. In this opportunity, it was evaluated the security aspect, through the corrosive study in a real combustion environment.

2. Methodology and materials

The applied methodology in this research work, was similar to one used by Alviz et al. (2017a) to study corrosion in a real combustion refinery environment.
The development of this work had an experimental and a simulation part. Simulation was useful to predict the possible corrosion products that could be obtained in the combustion environment worked. On the other hand, for experimental part execution, samples of P91 steel were introduced in a pirotubular horizontal boiler, whose only controlled variable was the exposure time of the samples.

2.1 Simulation

The first step to simulate theoretical corrosion products was to obtain the combustion gases composition. Then, the composition of the theoretical combustion products was simulated through Aspen HYSYS 8.6 software. Additionally, once having the experimental conditions, the composition of steel and combustion gases, to determine the theoretical corrosion products with HSC Chemistry 5.1 software was possible.

2.2 Experimental conditions

The boiler used for this corrosion study has ten years functioning, alternating between 12 h of continuous operation and 12 h out of service. Table 1 and Table 2 show another operating variables of the boiler.

Table 1: Boiler operating variables

Energy source	Air in excess	Operating pressure	Volumetric flow	Temperature
Natural gas	18 %	6.8 atm	24 m^3/h	850 ºC

Table 2: Molar natural gas composition used by the boiler

Compounds	CO_2	N_2	CH_4	C_2H_6	C_3H_8	i-C_4H_{10}	n-C_4H_{10}	i-C_5H_{12}	n-C_5H_{12}
%Molar	1.827	0.476	89.076	5.636	1.945	0.395	0.345	0.225	0.075

About the selected exposure times, given the equipment operation, they were taken in days (d). In that way, the implemented times were 1, 2, 5, 10 and 15 d. This means that in this work only the initial corrosive effects developed on P91 steel, in a real combustion environment, were studied. To introduce P91 samples in the boiler a coupons holder was use; in Figure 1 is possible to observe its capacity and disposition inside the boiler.

Figure 1: Back opening of the boiler, there the support of the samples is observed; which was located in front of the flame zone

This type of experimental conditions, typically correspond to studies of cyclic corrosion, because temperature does not remain uniform with time. Studies of this type have also been reported on Fe-9Cr-Mo alloys, as is the oxidation study carried out by Laverde et al. (2004), which can be used to discuss the results obtained in this work.

Regard to coupons preparation, through thread cutting technique, samples of 10 mm long, 15 mm high and 2 mm wide, were obtained. These samples were sanded before testing from SiC sandpaper No. 180 to 600. Each coupon was subjected to ultrasonic cleaning in acetone during 10 min, dried and marked, as is recommended by standard ASTM G1 (ASTM, 2011). To characterize the results SEM-EDS, XRD, hardness, microhardness and optical microscopy techniques were applied. Finally, the kinetic study was carried out taking into account the dimensions of the coupons, as well as the mass gained by each one.

3. Results

3.1 Simulation results

3.1.1 Determination of combustion environment

The theoretical combustion gases were simulated in Aspen HYSYS 8.6 software, taking into account the natural gas composition data and the percentage of excess air, previously detailed in Tables 1 and 2. The high percentage of free oxygen in the simulated combustion environment is an important result to highlight, as shown in Table 3.

Table 3: Molar combustion gases composition

Compounds	CO_2	N_2	O_2	H_2O
%Molar	8.30	72.73	3.37	15.60

3.1.2 Obtaining of theoretical corrosion products

Once determined the combustion molar composition at the experimental conditions, to obtain the equilibrium composition and phase stability diagrams were possible. Table 4 shows the elemental composition from the P91 supplied steel.

Table 4: Elemental weigh fraction of P91 steel

%Mo	%C	%Si	%Mn	%P	%S	%Ni	%Cr	%V	%Nb	%Al	%N	%Fe
0.989	0.106	0.768	0.316	0.013	0.003	0.271	8.439	0.024	0.008	0.006	0.015	89.042

According to the partial pressure of oxygen and carbon activity in the combustion environment, the phase stability diagrams were constructed. The bar in Figure 2 shows the range of values among which the carbon activity varies, between 550 and 850 ºC, for an oxidation potential of $pO_2 = 2.293 \times 10^{-1}\ atm$.

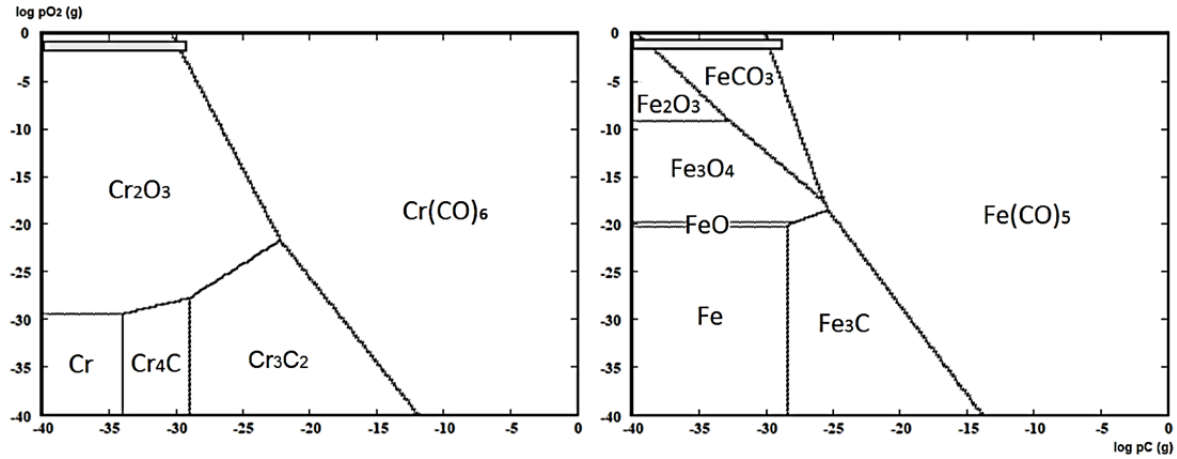

Figure 2: Cr-C-O and Fe-C-O phase stability diagrams from 550 to 850 °C

The regions between which the carbon activity moves, resulting in the possible formation of iron pentacarbonyl and chromium hexacarbonyl at 850 ºC. However, the formation of carbides is not predicted, for which a much lower oxygen potential would be needed in the environment.
Otherwise, thermodynamic equilibrium was also calculated, using the experimental conditions of pressure and temperature, as well as the steel and combustion gases composition. The molar steel/gas ratio used for this simulation in HSC Chemistry 5.1 was 1/1,000, as recommended by John (2010).
The main result indicated that carbide formation is not thermodynamically favoured but oxide formation does. The predominant oxides for the study conditions were: hematite (Fe_2O_3), magnetite (Fe_3O_4), chromite ($FeCr_2O_4$), goethite (FeO.OH), and silicon (SiO_2), Chromo (Cr_2O_3), Manganese (MnO_2) and molybdenum oxides (MoO_3), as well as the $FeMn_2O_4$ spinel.

3.2 Experimental results

3.2.1 Metallographic analysis

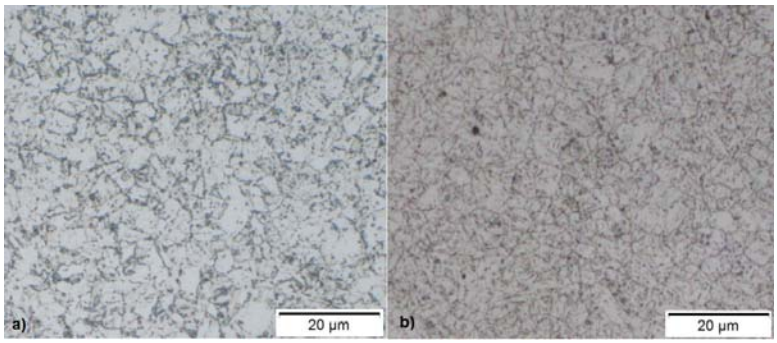

Figure 3: Cr-C-O Optical microscopy (500 x) for P91 steel: a) before testing and b) after 15 d at 850 °C

Through optical microscope, to study the P91 microstructure, before and after its exposure to experimental conditions was possible. Figure 3a, allows to appreciate a ferritic microstructure with a low content of lamellar perlite, with fine and coarse grain sizes; characteristic behaviour of normalized and tempered manufactured P91 steels. After 15 d at 850 ºC, P91 matrix shows also a ferritic microstructure with a smaller clumping of pearlite at the grain boundaries. This is a typical behaviour when the carbon diffusive processes in the alloys increase. This behaviour generates variations in the steel mechanical properties, reducing its resistance to stresses. In Figure 3b, is also possible to observe the formation of fine and thick carbide and carbonitrides precipitates; corresponding mainly to $M_{23}C_6$ and M_7C_6 carbides; with M as Cr, Fe, Mo, Nb and V.

3.2.2 Hardness and microhardness analysis

In order to complement the metallographic analyzes, physical hardness and microhardness tests were carried out. These results can be observed in Table 5.

Table 5: Hardness and microhardness analysis after 15 d at the experimental conditions. The force applied by each analysis was 588.40 and 0.49 N respectively

	Initial state	850 ºC
Hardness (Rockweel A)	58	55
Microhardness (Vickers HV)	229.4	190.8

The results of comparing the initial hardness of the steel with its hardness after the longer exposure time, did not show significant changes; which implies that there were no internal corrosion effects, as would be the case of carburization. Regarding the analysis of microhardness, a decrease was observed, which was related to the carbides diffusion throughout the alloy matrix.

3.2.3 Scanning electron microscopy with x ray microanalysis

As can be seen in Figure 4, a duplex oxide structure was found; composed mainly of an iron-rich outer layer and an inner layer rich in chromium. These results were also reported by Alviz et al. (2017b), Peña-Ballesteros et al. (2012), Martinelli et al. (2015) and Laverde et al. (2004). Additionally, Rouillard and Furukawa (2016) took the job of characterizing by TEM-EDS technique the innermost layer, finding that its composition

responds to the $Fe_{3-x}Cr_xO_4$ molecular formula. For its part, the outer layer has been reported as a layer rich in hematite and magnetite.

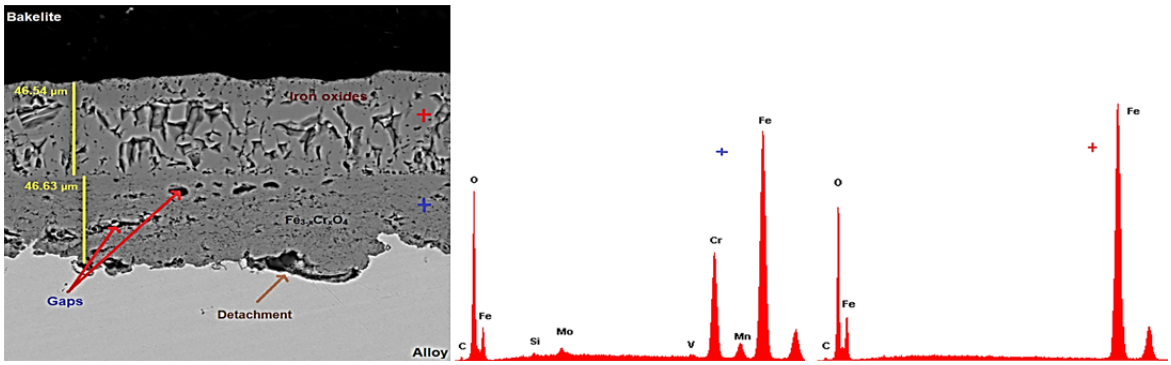

Figure 4: SEM-EDS after 15 d at 850 ºC (1,000 x)

An important aspect observed in Figure 4, is that, plus to the existence of multiple cracks, pores and voids through the oxides layers, there is also a detachment between the inner oxide layer and the alloy. This behaviour was also reported by Laverde et al. (2004) on Fe-9Cr-1Mo steel, during its cyclic oxidation in steam; where, due to the continuous efforts that are generated during the cooling-heating processes suffered by steel samples, the accelerated breakage of the oxide layer is induced.

A possible explanation for oxides layers behaviour, is based in the efforts theory proposed by Pilling-Bedworth. When ionic diffusion processes begins, dilation and compression efforts appears, which are related with the changing from a metallic crystalline structure to a cationic one. In this case, there are three oxide layers: an external hematite layer, an intermediate magnetite layer and an internal chromite layer; where, the stresses in each of them are described as follows. The layer of hematite develops compression efforts, so its failure is related to the buckling phenomenon. The magnetite layer generates tensile stresses, which contributes with its micro cracking behaviour. Finally, the internal layer generates compression efforts, which when added with diffusive processes, contribute to its plastic deformation. To this, the constant thermal expansions and multiple vacancies condensation are joined, producing finally the detachment of the metal oxide layer.

When the above process occurs, the chances to obtain corrosion by carburization increases, being that carbon-free atoms diffuse more easily towards the metallic matrix. However, for this to happen, longer exposure times are needed.

3.2.4 X-ray diffraction analysis

Through x-ray diffraction analysis, it was possible to determine the crystalline structures present at the oxide surface. So, it was only identified hematite (Fe_2O_3), magnetite (Fe_3O_4) and roaldite (Fe_4N). These results are consistent with the simulated combustion products; where carburization did not occur.

3.2.5 Kinetic study

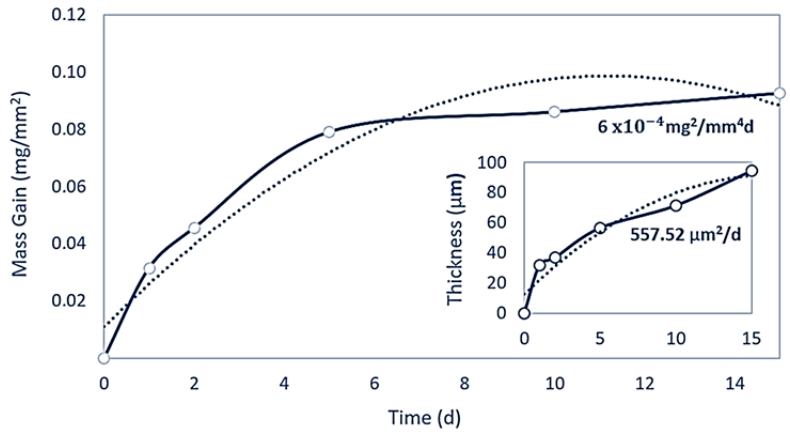

Figure 5: Thickness and mas gain against time, and parabolic kinetic constants. The dotted lines represent the parabolic trend

The kinetic study observed in Figure 5, allows to know the protective character of the oxide layers formed in the combustion environment. Thus, it was found that oxide layers do not have a perfectly parabolic behavior but is close to it. Such behavior is typical of oxide layers, where the diffusive processes slows down over time. When comparing the kinetic constants obtained in this work, with those reported by Laverde et al. (2004), a good similarity was found, although the experimental conditions were not so similar. These results are another indication that catastrophic oxidation wasn't presented, ruling out the formation of internal carbides or nitrides.

4. Conclusions

The main results of this work are reflected in the morphology analysis of the oxide layers obtained after 15 d at 850 ºC in a cyclic combustion environment. Of which, it can be said that: they were mainly composed of hematite (Fe_2O_3), magnetite (Fe_3O_4) and chromite ($FeCr_2O_4$), presenting efforts of compression, tension and compression; generating buckling, cracking and detachment respectively. These arguments are supported in the kinetic curves obtained, where the typical protective parabolic behaviour did not occur. Additionally, some localized surface nitridation (Fe_4N) was also identified, but no carburization effects; the oxygen partial pressure ($pO_2 = 2.293 \times 10^{-1}\ atm$) was high enough to suppress its effect. Finally, the metallographic analysis showed a ferritic structure with fine pearlite grains, as well as, the precipitation of carbides type $M_{23}C_6$ and M_7C_6 in the metallic matrix, which spread throughout the alloy with the constant thermal treatments.

Acknowledgments

The authors expressed their acknowledgments to the Administrative Department of Science, Technology and Innovation of Colombia (COLCIENCIAS) and Colombian Network of Knowledge in Energy Efficiency (RECIEE) for financial support of this work that is part of the project "Consolidation of the knowledge network on energy efficiency and its impact on the productive sector under international standards - Design of a methodology for the eco-efficient management of combustion processes, case study: the oil refining industry" code of COLCIENCIAS: 110154332086.

References

Alviz, A., Kafarov, V., Meriño L., 2017, Methodology for evaluation of corrosion damage during combustion process in refinery and petrochemical industry. case study: AISI 304 and astm A335 P5 steels, Chemical Engineering Transactions, 61, 1315-1320.

Alviz, A., Kafarov, V., Peña-Ballesteros, D., 2017, Study of the continuous corrosion in an oxidation environment derived from the theoretical combustion products in a refinery. Case study: Ferritic steel ASTM A335 P91, IOP Conf. Series: Journal of Physics, 935, 1-7.

ASTM (American Society for Testing and Materials), 2011. Standard Practice for Preparing, Cleaning, and Evaluating Corrosion Test Specimens (ASTM G1-03 ed.). United States: ASTM International.

Fabricius, A., Jackson, P., 2016, Premature grade 91 failures - worldwide plant operational experiences, Engineering Failure Analysis, 66, 398–406.

Ju, G.Z., Wu, W.Z., Dai, S.H., 1997, Failure of 9Cr-1Mo tubes in a feed furnace of dehydrogenation unit, International Journal of Pressure Vessels and Piping, 74, 199-204.

John, R., 2010, Sulfidation and mixed gas corrosion of alloys. Shreir's Corrosion, 240–271.

Kafarov, V., Toledo, M., Meriño, L., 2015, Numerical Simulation of Combustion Process of Fuel Gas Mixtures at Refining Industry, Chemical Engineering Transactions, 43, 1351–1356.

Laverde, D., Gómez-acebo, T., Castro, F., 2004, Continuos and cyclic oxydation of T91 ferritic steel under steam, Corrosion science, 46, 613-631.

Martinelli, L., Desgranges, C., Rouillard, F., Ginestar, K., Tabarant, N., Rousseau, K., 2015, Comparative oxidation behaviour of Fe-9Cr steel in CO_2 and H_2O at 550ºC: Detailed analysis of the inner oxide layer, Corrosion Science, 100, 253-266.

Peña-Ballesteros, D., Vásquez-Quintero, C., Laverde-Cataño, D., Serna-Gil, A., 2012, High temperature corrosion of 9Cr-1Mo ferritic steel P91 modified, in oxidizing-carburizing atmospheres, Revista de Metalurgia, 48, 97-106. [In Spanish]

Rouillard, F., Furukawa, T., 2016, Corrosión of 9-12Cr ferritic-martensitic steels in high temperature CO_2, Corrosion Science, 105, 120–132.